NONUNIFORM TORSION WITHOUT SHEAR DEFORMATION EFFECT USING FEM

Dang-Bao TRAN[1,2], *Jaroslav NAVRÁTIL*[1]

[1] Department of Structures, Faculty of Civil Engineering, VSB–Technical University of Ostrava, Ludvíka Podéště 1875/17, Ostrava, Czech Republic.
[2] Department of Civil Engineering, Faculty of Architecture, Thu Dau Mot University, Tran Van On 06, Binh Duong Province, Vietnam.

dang.bao.tran@vsb.cz, jaroslav.navratil@vsb.cz.

DOI: 10.35181/tces-2021-0006

Abstract. *This paper presents the use of a finite element method (FEM) to analyze nonuniform torsion with an arbitrary cross-section with homogeneous elastic material without shear deformation effect. Beams are constrained by the most common types of supports, such as fixed, pinned, and roller, and are subjected to any applied torsional load, concentrated, and distributed. The presented FEM transforms the 3D analysis of nonuniform torsion beams into separated 2D cross-sectional and 1D modeling. The geometric constants of the cross-section are firstly derived from 2D FEM, which uses a 9-node isoparametric element. Then, a 1D FEM, which uses the Hermitian shape function, is developed for computing the twist angle, the derivative of twist angle, and stress resultants. Finally, the stress field is obtained from the local analysis on the 2D-cross section. A MATLAB program is executed to validate the numerical method through examples. The validation examples have proven the reliability of the author's numerical method for analyzing problems defined above.*

Keywords

Nonuniform torsion, thin-walled structure, shear deformation effect, warping restraint, finite element method.

1. Introduction

In engineering practice, we often encounter beam structures loaded in torsion. When the warping of a member's cross-section is not restrained, the stress field of a prismatic beam with homogeneous isotropic material can be derived from the Saint-Venant theory strictly [1-4]. In practice, because i) boundary conditions are imposed, ii) geometrical characteristics of the section, the warping of beam's cross-section is restrained, which leads to additional normal and shear stresses, which the Saint Venant theory does not take into account. Vlasov [5] was the first to formulate the problem of nonuniform torsion. Benscoter [6] improved Vlasov's theory, which neglects the shear deformation effect, leading to errors with closed cross-sections [7].

Many authors established FEM to consider nonuniform torsion taking into account the shear deformation effect [7-14]. However, the above research [7-14] used the approximations of Thin Tube Theory [5] to determine the bar's geometric constants, restricting the accuracy and applicability of the formulations. El Fatmi [15,16] proposed a beam theory with a nonuniform warping, including the effects of torsion and shear forces for arbitrary cross-sections made of homogeneous isotropic elastic material. Mokos and Sapountzakis [17] presented a nonuniform torsion theory considering the shear deformation effect for general cross-sections implemented by Boundary Element Method. The purpose of this paper is to establish a numerical method using FEM to solve the nonuniform torsion problem without the shear deformation effect of the prismatic beam with arbitrary cross-section unchanged throughout the length with homogeneous isotropic elastic material, based on displacement and strain fields derived from Sapountzakis, EJ et al. [17]. This paper is a preliminary research step for future research, which considers the shear deformation effect in nonuniform torsion.

2. A brief introduction of the theoretical formulas for nonuniform torsion

Let us consider a prismatic beam with arbitrary cross-section, constant along the length L with the modulus of elasticity E, and shear modulus G. The longitudinal axis is the x-axis, and the cross-sections lie in the y–z plane. S is the shear center of the cross-section. The parallel system $\overline{z} = z + \overline{z}_S$, $\overline{y} = y + \overline{y}_S$ intersects at O, the arbitrary point. $CXYZ$ is the parallel system with $Sxyz$ through the center

of gravity *C*.

The multiply connected domain Ω is bounded by n curves, Γ_1, Γ_2, ..., Γ_{n-1}, Γ_n, as Fig. 1. Tangent vector **t** with associate coordinate **s** and normal vector **n** set up the right-handed system. The beam is enforced to the arbitrary loads, distributed torque $m_t(x)$, concentrated torque $M_{ti}(x)$, concentrated warping moment $M_{wi}(x)$. The cross-section is assumed with no distortion.

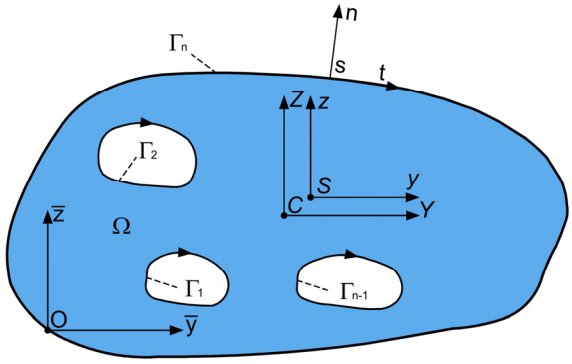

Fig. 1: Cross-section of the prismatic beam

The displacement field is expressed as [17]

$$u(x,y,z) = \theta_x'\phi_S^P(y,z) + \phi_S^S(y,z), \tag{1}$$

$$v(x,z) = -z\theta_x(x), \tag{2}$$

$$w(x,y) = y\theta_x(x), \tag{3}$$

where *u, v, w* are the axial and transverse displacements of the beam with respect to *Sxyz*

θ_x is the angle of twist

$\phi_S^P(y,z)$ is the primary warping function with respect to shear center *S* derived from

$$\begin{aligned} &\nabla^2\phi_S^P = 0 \text{ in } \Omega \\ &\frac{\partial\phi_S^P}{\partial y}n_y + \frac{\partial\phi_S^P}{\partial z}n_z = zn_y - yn_z \text{ on } \Gamma_n. \end{aligned} \tag{4}$$

Moreover, the restrained warping function can be computed as follows by using the transformation of coordinates [18]

$$\phi_S^P(y,z) = \phi_O^P(\bar{y},\bar{z}) + \bar{y}_S Z - \bar{z}_S Y - \frac{1}{A}\int_\Omega \phi_O^P(\bar{y},\bar{z})dA. \tag{5}$$

where $\phi_O^P(\bar{y},\bar{z})$ is the warping function with respect to $O\bar{y}\bar{z}$ system coordinates, *A* is the area of the cross-section

ϕ_S^S is the secondary warping function with respect to the shear center *S*, given as

$$\begin{aligned} &\nabla^2\phi_S^S = -\frac{E\theta_x'''(x)}{G}\phi_S^P \text{ in } \Omega \\ &\frac{\partial\phi_S^S}{\partial y}n_y + \frac{\partial\phi_S^S}{\partial z}n_z = 0 \text{ on } \Gamma_n, \end{aligned} \tag{6}$$

The stress fields obtained from the theory of elasticity as [17]

$$\sigma_{xx} = E\theta_x''(x)\phi_S^P(y,z), \tag{7}$$

$$\tau_{xy} = \underbrace{G\theta_x'(x)\left(\frac{\partial\phi_S^P}{\partial y} - z\right)}_{\tau_{xy}^P} + \underbrace{G\frac{\partial\phi_S^S}{\partial y}}_{\tau_{xy}^S}, \tag{8}$$

$$\tau_{xz} = \underbrace{G\theta_x'(x)\left(\frac{\partial\phi_S^P}{\partial z} + z\right)}_{\tau_{xz}^P} + \underbrace{G\frac{\partial\phi_S^S}{\partial z}}_{\tau_{xz}^S}, \tag{9}$$

In addition, the shear stress in (8), (9) can be seen as composed of two parts: primary shear stress and secondary shear stress.

The warping moment, the total twisting moment, the primary twisting moment, the secondary twisting moment are denoted by M_w, M_t, M_t^P, M_t^S obtained as [17]

$$M_w = -\int_\Omega \sigma_{xx}\phi_S^P d\Omega = -EC_S\theta_x''', \tag{10}$$

$$\begin{aligned} M_t^P &= \int_\Omega \left[\tau_{xy}^P\left(\frac{\partial\phi_S^P}{\partial y} - z\right) + \tau_{xz}^P\left(\frac{\partial\phi_S^P}{\partial z} + y\right)\right]d\Omega \\ &= GI_t\theta_x', \end{aligned} \tag{11}$$

$$M_t^S = \int_\Omega \left(-\tau_{xy}^S\frac{\partial\phi_S^P}{\partial y} - \tau_{xz}^S\frac{\partial\phi_S^P}{\partial z}\right) = -EC_S\theta'''(x), \tag{12}$$

$$M_t = M_t^P + M_t^S, \tag{13}$$

where I_t is the torsional constant, determined as

$$I_t = \int_\Omega \left(y^2 + z^2 + y\frac{\partial\phi_S^P}{\partial z} - z\frac{\partial\phi_S^P}{\partial y}\right)d\Omega, \tag{14}$$

C_S are the warping constant determined by

$$C_S = \int_\Omega \left(\phi_S^P\right)^2 d\Omega. \tag{15}$$

The relation between the stress resultant, total twist moment M_t, and the distributed torque $m_t(x)$ is expressed as [17]

$$\frac{\partial M_t}{\partial x} = -m_t(x). \tag{16}$$

After some algebra, the equilibrium equation for the nonuniform torsion problem of a homogeneous isotropic bar without shear deformation effect is expressed as

$$EC_S\frac{d^4\theta_x}{dx^4} - GI_t\frac{d^2\theta_x}{dx^2} = m_t. \tag{17}$$

3. FEM procedures

3.1. Angle twist, θ_x

Applying Galerkin's method, one of the methods of weighted residual, the governing equation Eq. (17) is transformed to weak form as

$$I = \int_0^L \left(EC_S \frac{d^4\theta_x}{dx^4} - GI_t \frac{d^2\theta_x}{dx^2} - m_t \right) \eta dx = 0, \tag{18}$$

where η is the test function.

The beam is discretized into a number of finite elements. After some manipulation, the weak formulation of Eq. (18) can be expressed as

$$I = \sum_{i=1}^{n} \left[\int_{L_e} EC_S \frac{d^2\theta_x}{dx^2} \frac{d^2\eta}{dx^2} dx + \int_{L_e} GI_t \frac{d\theta_x}{dx} \frac{d\eta}{dx} - \int_{L_e} m_t \eta dx \right] + \left[-GI_t \frac{d\theta_x}{dx} \eta + M_t \frac{d\eta}{dx} - M_w \frac{d\eta}{dx} \right]_0^L = 0, \tag{19}$$

where

L_e is an beam element domain

n is the number of elements for the beam.

The Hermitian polynomial interpolation function, which achieves the correct solution of the problem with refining mesh, proves more flexible than the Hyperbolic interpolation function, which gives the most accurate results with the most analytical solution [19]. We choose cubic functions for the spatial interpolation of the twist angle, θ_x, in terms of nodal variables. To this end, we consider an element that has two nodes, one at each end. The twist angle can be expressed as

$$\theta_x = H_1(x)\theta_{x1} + H_2(x)\frac{d\theta_{x1}}{dx} + H_3(x)\theta_{x2} + H_4(x)\frac{d\theta_{x2}}{dx}, \tag{20}$$

where

$$H_1(x) = 1 - \frac{3x^2}{l^2} + \frac{2x^3}{l^3}, \quad H_2(x) = x - \frac{2x^2}{l} + \frac{x^3}{l^3}, \quad H_3(x) = \frac{3x^2}{l^2} - \frac{2x^3}{l^3}, \quad H_4(x) = -\frac{x^2}{l^2} + \frac{x^3}{l^3}, \tag{21}$$

$\theta_{x1}, \frac{d\theta_{x1}}{dx}, \theta_{x2}, \frac{d\theta_{x2}}{dx}$ are the nodal degrees of freedom.

Inserting the Eq. (20), Eq. (21) to Eq. (19) results in the stiffness matrix of the beam element

$$\mathbf{K} = \mathbf{K}_1^e + \mathbf{K}_2^e, \tag{22}$$

where

$$\mathbf{K}_1^e = EC_S \int_0^{L_e} \mathbf{B}_1^T \mathbf{B}_1 dx, \tag{23}$$

$$\mathbf{K}_2^e = GI_t \int_0^{L_e} \mathbf{B}_2^T \mathbf{B}_2 dx, \tag{24}$$

where

$$\mathbf{B}_1 = \left[\frac{d^2H_1}{dx^2} \quad \frac{d^2H_2}{dx^2} \quad \frac{d^2H_3}{dx^2} \quad \frac{d^2H_4}{dx^2} \right], \tag{25}$$

$$\mathbf{B}_2 = \left[\frac{dH_1}{dx} \quad \frac{dH_2}{dx} \quad \frac{dH_3}{dx} \quad \frac{dH_4}{dx} \right]. \tag{26}$$

The corresponding element nodal degrees of freedom is $\mathbf{d^e} = \left\{ \theta_{x1}, \frac{d\theta_{x1}}{dx}, \theta_{x2}, \frac{d\theta_{x2}}{dx} \right\}^T$. (27)

The third term in Eq.(19) results in the element force vector. For a generally distributed torque, we need to compute

$$\mathbf{F^e} = \int_0^{L_e} m_t(x) \begin{Bmatrix} H_1 \\ H_2 \\ H_3 \\ H_4 \end{Bmatrix} dx, \tag{28}$$

where $\mathbf{F^e}$ is the element force vector.

The last term in Eq. (19) is the boundary conditions of the total twisting moment and the warping moment at the two boundary points, $x = 0$ and $x = L$, of the beam. If these boundary conditions are known, the known total twisting moment and warping moment are included in the system force vector at the two boundary nodes. Otherwise, they remain unknown. However, the twist angle and the derivative of the twist angle are known as geometric for this case. Assembling the element stiffness matrix and vectors leads to the system matrix equation given below

$$\mathbf{Kd} = \mathbf{F}. \tag{29}$$

3.2. Warping function, ϕ_S^P, ϕ_S^S

Using Galerkin's method, with test function $\eta \in H^1(\Omega)$ and applying the Gauss-Green theorem, the governing equations Eq. (4), Eq. (6) are transformed to weak form as

$$\int_\Omega \left(\frac{\partial \phi_S^P}{\partial y} \frac{\partial \eta}{\partial y} + \frac{\partial \phi_S^P}{\partial z} \frac{\partial \eta}{\partial z} \right) d\Omega - \oint_{\Gamma_n} (n_y z - n_z y) \eta ds = 0. \tag{30}$$

$$\int_\Omega \left(\frac{\partial \phi_S^S}{\partial y} \frac{\partial \eta}{\partial y} + \frac{\partial \phi_S^S}{\partial z} \frac{\partial \eta}{\partial z} \right) d\Omega - \int_\Omega \left(\frac{E\theta_x'''(x)}{G} \right) \phi_S^P \eta d\Omega = 0. \tag{31}$$

The warping function values, ϕ_S^P, ϕ_S^S, in Eq. (30) and Eq. (31) are approximated by the FEM, which is presented in [3, 4].

4. Validation examples

In this section, the accuracy of the proposed FEM has been examined. A computer code is developed in the MATLAB R2015a software based on the formulations described in the previous sections. The obtained results are compared with the available works of the literature.

4.1. Example 1

As a first example, a thin-walled beam with an I-shaped cross-section shown in Fig. 2 is analyzed and compared with the results obtained by Tralli, A.M. [8] and Kim, N. I. et al. [11]. The I-section beam is clamped–free and the concentrated torsional moment $M_x = 25$ kNm is applied at its free end. The length of the beam is 5 m. The Young's modulus and the Poisson's ratio are $E = 2$ x 10^6 MPa and $\nu = 0.3$, respectively. The first test was analyzed using 16 axial elements and 19 elements in the cross-section. The geometric constants of the cross-section determined from the present study are as follows $C_S = 2.1559\times10^{-7}\,m^6$, $I_t = 2.8643\times10^{-6}\,m^4$.

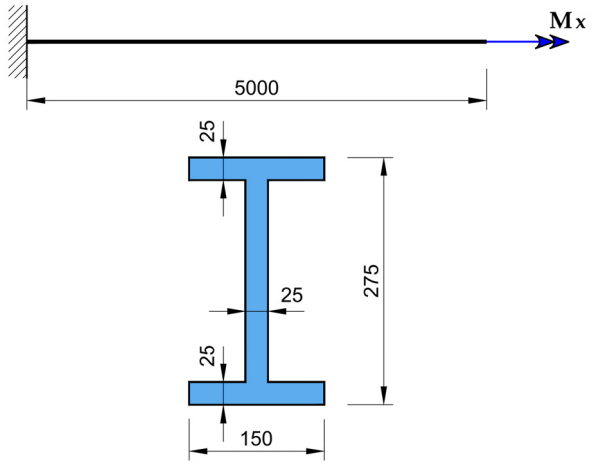

Fig. 2: A cantilever beam, the applied load, and the geometry of the I cross-section, units [mm].

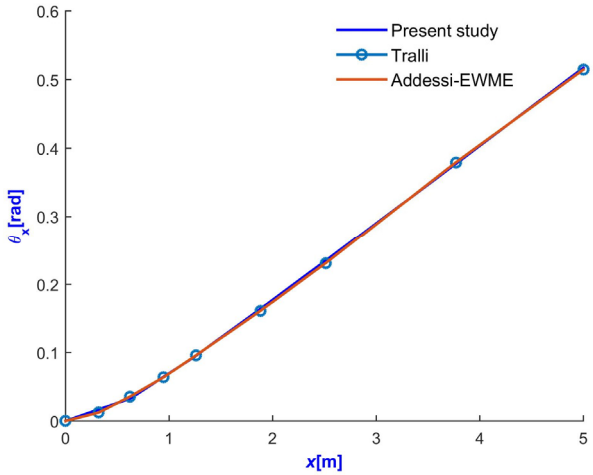

Fig. 3: The variation of twist angle along the x-axis.

In Table 1, the angle of twist at the free end predicted by the present study is given and compared with the results of other researchers. The variations of the angle of twist along the length of the thin-walled beam are shown in Fig. 3. It can be seen from Table 1 and Fig. 3 that the twist angle results obtained from the present study are in excellent agreement with other works.

Tab.1: Comparison of the twist angle θ_x at the free end calculated by different methods

Methods	θ_x $[rad]$ at x = L
Present study	0.5171
Tralli [8]	0.5183
Kim et al [11]	0.5173
Vlasov [11]	0.5167

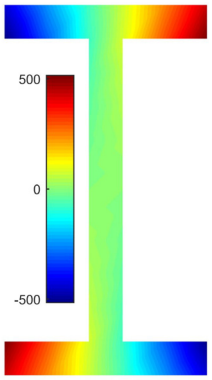

Fig. 4: Distribution of the axial stress σ_{xx} in 2D cross-section at fix-end, unit MPa,

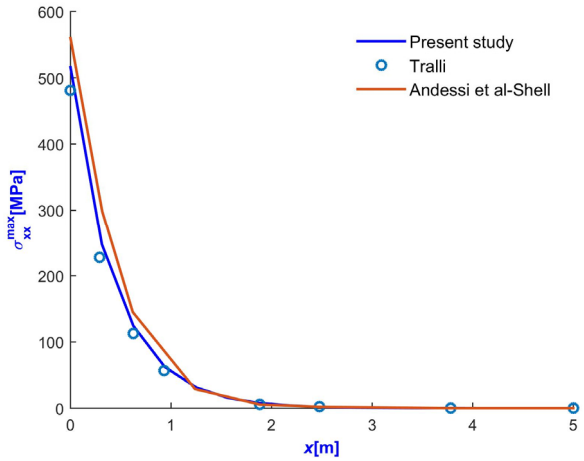

Fig. 5: Maximum of normal stress σ_{xx} along the axis x of the beam.

Fig. 4 shows the contour plot of the axial stress σ_{xx} at the clamped end of the I-section beam. Fig. 5 depicts the variation along the axis x of the normal stress σ_{xx}. Fig. 6 and Fig. 7 present the variation along the axis x of the warping moment and the torsional moments, respectively. It is observed from Fig. 4 that the variations of the axial stress are symmetric to the area center of the cross-section. In contrast to the flanges, no significant axial stress appears at the web of the I-section beam. The maximum value of σ_{xx} = 515.911 MPa occurs at the corners of the

flanges. In Fig. 5, the variations of the maximum axial stress σ_{xx} at the fixed-end of the cross-section along the length of the beam are shown and compared to the ones obtained from [8, 11]. It can be seen that the axial stress predicted by the present study is in good agreement with the results of Tralli, A. M. [8].

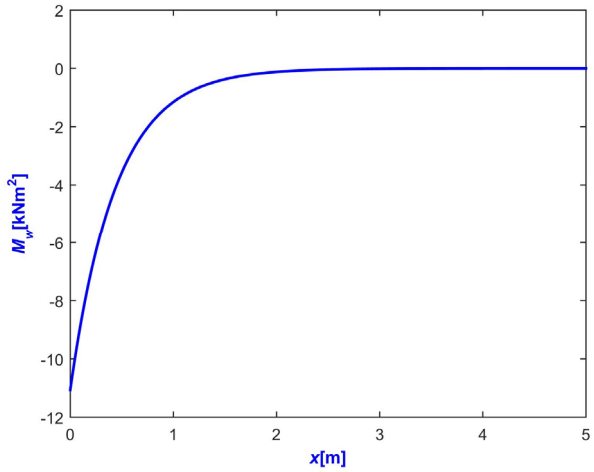

Fig. 6: The variation of warping moment M_w along the axis x of the beam.

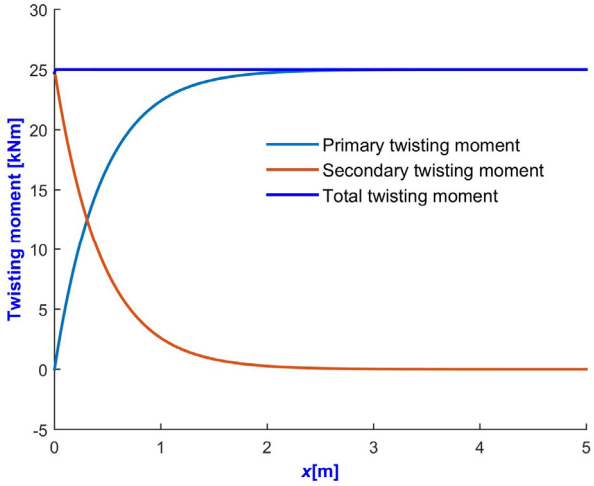

Fig. 7: The variation of torsional moments along the axis x of the beam.

4.2. Example 2

A cantilevered thin-walled beam with a channel cross-section depicted in Fig.8 is analyzed in this section. The depth, width, and thickness of the cross-section are h = 0.833 m, b = 0.917 m, t = 1/6 m, respectively. The length of the beam is L = 4 m and, it is made of a material with the modulus of elasticity E = 2 x 10^5 MPa and the shear modulus G = 0.77 x 10^5 MPa. The considered thin-walled beam is subjected to uniformly distributed twisting moment equal to m_x = 4.07 x 10^3 kNm/m. The second example was analyzed using in the present study by employing 80 axial elements and 64 elements in the cross-section. The geometric constants of the cross-section determined from the present study are as follows $C_S = 0.0059m^6$, $I_t = 0.00407889m^4$.

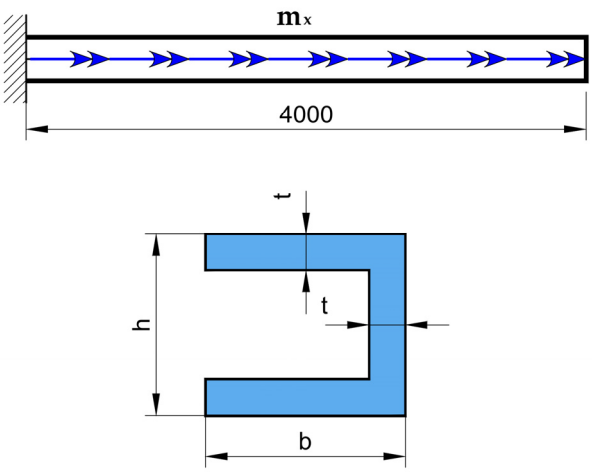

Fig. 8: Cantilever beam, the applied load, and the geometry of the channel cross-section, units [mm].

Shakourzadeh, H. et al. [7] used FEM based on Benscoter's model to solve this problem and compared it with the results obtained from Vlasov's theory, which neglects the shear deformation effect. Meanwhile, Sapountzakis, E. J. et al. [20] used Analog Equation Method (AEM) and AEM with isogeometric analysis with 3 B-spline types: i) Quadratic B-spline, ii) Cubic B-spline), iii) Quadratic B-spline to investigate this problem.

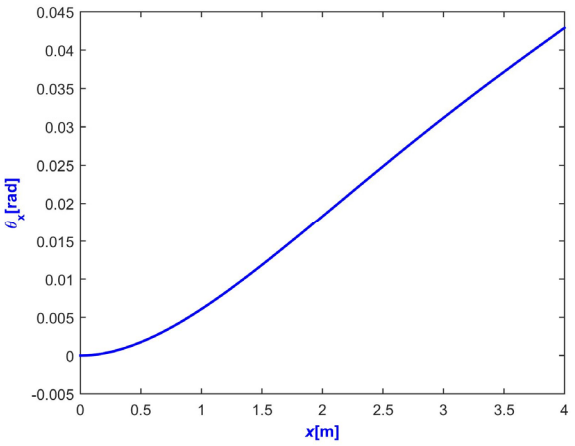

Fig. 9: The variation of twist angle along the x-axis.

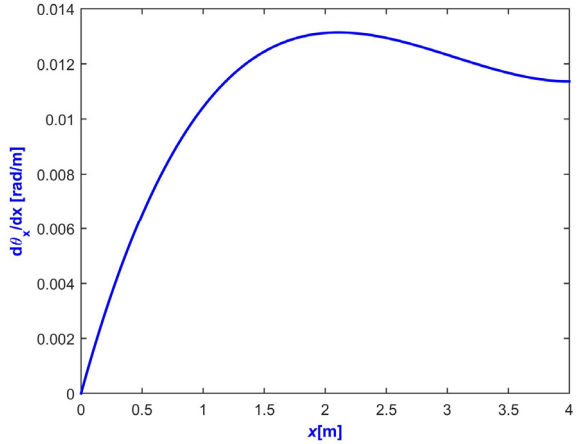

Fig. 10: The variation of derivative of the twist angle along the x-axis.

Fig. 9 and Fig.10 show the variation of the angle of twist and the derivative of twist angle along the *x*-axis, respectively. The value of the angle of twist and the derivative of twist angle at the free end, and the warping moment at the fixed end are presented in Table 2 and compared with the ones obtained from Shakourzadeh, H. et al [7], Sapountzakis, E. J. et al. [20].

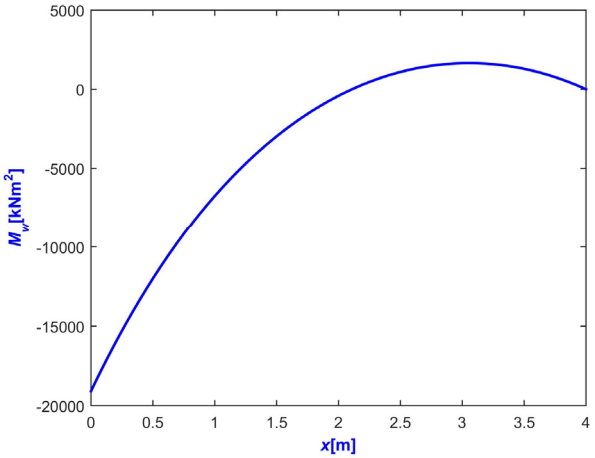

Fig. 11: The variation of warping moment along the *x*-axis.

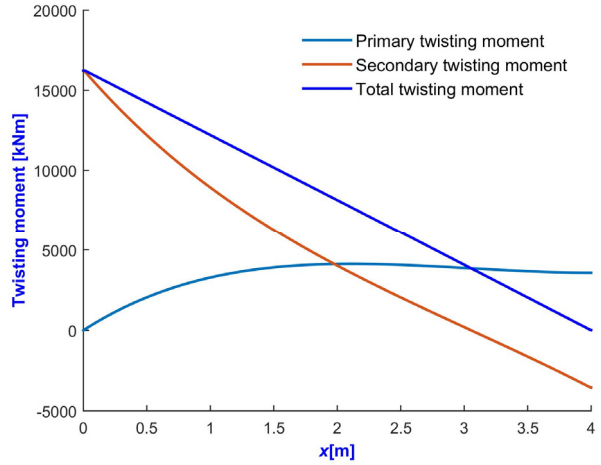

Fig. 12: The variation of the torsional moment along the *x*-axis.

Tab.2: Comparison of the twist angle, the derivative of twist angle, and warping moment between the methods

Methods	θ_x [rad] at x = L	θ_x' [rad/m] at x = L	Warping moment M_w [N.m^2] at x = 0
Present study	-0.0429	-0.0114	-19.083 x 10^6
Saint- Venant model [7]	-0.103	-	-
Vlasov model [7]	-0.045	-0.012	-18.33 x 10^6
FEM-Benscoter model [7]	-0.045	-0.011	-18.17 x 10^6
AEM (50NP) [20]	-0.050	-0.009	-16.75 x 10^6
AEM(Quadratic B-spline) [20]	-0.039	-0.006	-13.48 x 10^6
AEM(Cubic B-spline) [20]	-0.061	-0.013	-18.29 x 10^6
AEM(Quaratic B-spline) [20]	-0.046	-0.008	-15.5 x 10^6

Fig. 11 and Fig.12 depict the variation of the warping moment and the torsional moments along the axis, respectively. It can be seen from Table 2 that the twist angle analyzed by the present study is in good agreement with the results of Vlasov model [7], FEM-Benscoter model [7], and AEM(Cubic B-spline) [20].

The distribution of the axial stress σ_{xx} and shear stress τ_{xy} inside the channel cross-section at the position x = 0.5 m is shown in Fig. 13. The maximum normal stress σ_{xx} = 657.865 MPa occurs on the tip of the flange. As expected, the distribution of the shear stress τ_{xy}, with the maximum value 205.981 MPa, decreases from the outer flange edge to the inner edge [21].

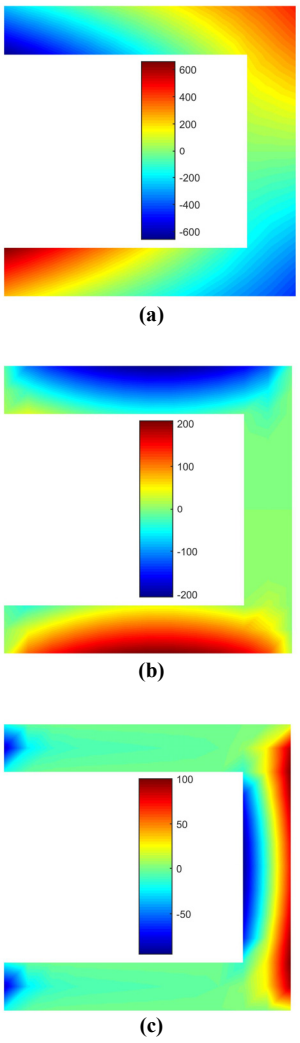

Fig. 13: The normal stress σ_{xx} and b) the shear stress τ_{xy} b) the shear stress τ_{xz} at x = 0.5 m from the fixed-end, units [MPa].

5. Conclusion

In this paper, a finite element method is developed to solve nonuniform torsion without the shear deformation effect of the prismatic beam with an arbitrary cross-section with homogeneous isotropic material. Two examples were performed for validating the accuracy of the present study.

The comparison of the results from the present study with the corresponding results in the literature shows that the present study can predict the responses of the non-uniform torsion with arbitrary cross-section without shear deformation effect accurately. Linear analysis of nonuniform torsion considering shear deformation would be one of the future research topics.

Acknowledgments

The works were supported by the Student Grant Competition VSB-TUO. The registration number of the project is SP2021/77 “Nonuniform torsion in prismatic beams with arbitrary cross-sections using FEM”.

References

[1] TIMOSHENKO, S. P and J. N. GOODIER. *Theory of elasticity*. New York, USA: McGraw-Hill Book Company, 1951.

[2] PILKEY, W. D. *Analysis and design of elastic beams: Computational methods*. New York, USA: John Wiley & Sons, 2002. ISBN: 0-471-38152-7.

[3] TRAN, D. B., J. NAVRÁTIL and M. ČERMÁK. An efficiency method for assessment of shear stress in prismatic beams with arbitrary cross-sections. *Sustainability (Switzerland)*. 2021. Vol. 13, no. 2, pp. 1–20. ISSN 20711050. DOI: 10.3390/su13020687.

[4] TRAN, D.-B. Torsional Shear Stress in Prismatic Beams With Arbitrary Cross-Sections Using Finite Element Method. *Stavební obzor - Civil Engineering Journal*. 2021. Vol. 30, no. 2. ISSN 1805-2576. DOI: 10.14311/cej.2021.02.0030.

[5] VLASOV, V. Z. Thin walled elastic beams. Israel Program for Scientific Translations. *Jerusalem, Israel*. 1961.

[6] BENSCOTER, S. U. A Theory of Torsion Bending for Multicell Beams. *Journal of Applied Mechanics*. 1954. Vol. 21, no. 1, pp. 25–34. ISSN 0021-8936. DOI: 10.1115/1.4010814.

[7] SHAKOURZADEH, H., Y. Q. GUO and J. L. BATOZ. A torsion bending element for thin-walled beams with open and closed cross sections. *Computers and Structures*. 1995. Vol. 55, no. 6, pp. 1045–1054. ISSN 00457949. DOI: 10.1016/0045-7949(94)00509-2.

[8] TRALLI, A. A simple hybrid model for torsion and flexure of thin-walled beams. *Computers and Structures*. 1986. Vol. 22, no. 4, pp. 649–658. ISSN 00457949. DOI: 10.1016/0045-7949(86)90017-9.

[9] BACK, S. Y. and K. M. WILL. A shear-flexible element with warping for thin-walled open beams. *International Journal for Numerical Methods in Engineering*. 1998. Vol. 43, no. 7, pp. 1173–1191. ISSN 00295981. DOI: 10.1002/(SICI)1097-0207(19981215)43:7<1173::AID-NME340>3.0.CO;2-4.

[10] Erkmen, R.E. and M. Mohareb. Torsion analysis of thin-walled beams including shear deformation effects. *Thin-walled structures*. 2006. Vol. 44, no. 10, pp.1096-1108. ISSN 0263-8231. DOI: 10.1016/j.tws.2006.10.012.

[11] KIM, N. I. and M. Y. KIM. Exact dynamic/static stiffness matrices of non-symmetric thin-walled beams considering coupled shear deformation effects. *Thin-Walled Structures*. 2005. Vol. 43, no. 5, pp. 701–734. ISSN 02638231. DOI: 10.1016/j.tws.2005.01.004.

[12] MURÍN, J. and KUTIŠ, V. An effective finite element for torsion of constant cross-sections including warping with secondary torsion moment deformation effect. *Engineering Structures*. 2008. Vol. 30, no. 10, pp. 2716–2723. ISSN 01410296. DOI: 10.1016/j.engstruct.2008.03.004.

[13] MURÍN, J., V. KUTIŠ, V. KRÁLOVIČ and T. SEDLÁR. 3D beam finite element including nonuniform torsion. *Procedia Engineering*. 2012. Vol. 48, p. 436–444. ISSN 18777058 DOI: 10.1016/j.proeng.2012.09.537.

[14] MURÍN, J., M. AMINBAGHAI, V. KUTIŠ, V. KRÁLOVIČ, T. SEDLÁR, V. GOGA and H. MANG. A new 3D Timoshenko finite beam element including non-uniform torsion of open and closed cross sections. *Engineering Structures*. 2014. Vol. 59, pp. 153–160. ISSN 01410296. DOI: 10.1016/j.engstruct.2013.10.036.

[15] EL FATMI, R. Non-uniform warping including the effects of torsion and shear forces. Part I: A general beam theory. *International Journal of Solids and Structures*. 2007. Vol. 44, no. 18–19, pp. 5912–5929. ISSN 0020-7683. DOI: 10.1016/j.ijsolstr.2007.02.006.

[16] EL FATMI, R. Non-uniform warping including the effects of torsion and shear forces. Part II: Analytical and numerical applications. *International Journal of Solids and Structures*. 2007. Vol. 44, no. 18–19, pp. 5930–5952. ISSN 00207683. DOI: 10.1016/j.ijsolstr.2007.02.005.

[17] SAPOUNTZAKIS, E. J. Bars under Torsional Loading: A Generalized Beam Theory Approach. *ISRN Civil Engineering*. 2013. Vol. 2013, pp. 1–39. ISSN 2090-5114. DOI: 10.1155/2013/916581.

[18] GRUTTMANN, F., R. SAUER and W. WAGNER. Shear stresses in prismatic beams with arbitrary cross-sections. *International Journal for Numerical Methods in Engineering*. 1999. Vol. 45, no. 7, pp. 865–889. ISSN 00295981. DOI: 10.1002/(SICI)1097-0207(19990710)45:7<865::AID-NME609>3.0.CO;2-3.

[19] MOHAREB, Magdi and F. NOWZARTASH. Exact Finite Element for Nonuniform Torsion of Open Sections. *Journal of Structural Engineering*. 2003. Vol. 129, no. 2, pp. 215–223. ISSN 0733-9445. DOI: 10.1061/(asce)0733-9445(2003)129:2(215).

[20] SAPOUNTZAKIS, E. J. and I. N. TSIPTSIS. B-splines in the Analog Equation Method for the generalized beam analysis including warping effects. *Computers and Structures*. 2017. Vol. 180, pp. 60–73. ISSN 00457949. DOI: 10.1016/j.compstruc.2016.03.007.

[21] GENOESE, A. et al. A mixed beam model with non-uniform warpings derived from the Saint Venànt rod. *Computers & Structures*. 2013. Vol. 121, p. 87–98. ISSN 0045-7949. DOI: 10.1016/j.compstruc.2013.03.017.